Biocidal Activity of Low Temperature Plasma to Xylella Fastidiosa

Paolo F. Ambrico (paolofrancesco.ambrico@cnr.it)
National Research Council of Italy - Institute for Plasma Science and Technology
Stefania Zicca
National Research Council of Italy - Institute for Sustainable Plant Protection
Marianna Ambrico
National Research Council of Italy - Institute for Plasma Science and Technology
Palma R. Rotondo
University of Bari ALDO MORO - Department of Soil, Plant and Food Sciences
Angelo Stradis
National Research Council of Italy - Institute for Sustainable Plant Protection
Maria Saponari
National Research Council of Italy - Institute for Sustainable Plant Protection
Donato Boscia
National Research Council of Italy - Institute for Sustainable Plant Protection
Pasquale Saldarelli
National Research Council of Italy - Institute for Sustainable Plant Protection

Research Article

Keywords: Xylella fastidiosa, plasma, high decontamination, XfDD cells, Philaenus spumarius

Posted Date: September 20th, 2021

DOI: https://doi.org/10.21203/rs.3.rs-886549/v1

Abstract

The quarantine bacterium *Xylella fastidiosa* was first detected in Salento (Apulia, Italy) in 2013 and caused severe symptoms in olives, leading to plant death. The disease, named Olive Quick Decline Syndrome (OQDS), is caused by the strain "De Donno" ST53 of the subspecies *pauca* of this bacterium (XfDD), which is spread by *Philaenus spumarius*. The epidemic poses a serious threat to the agricultural economy and the landscape, as *X. fastidiosa* infects several plant species and there is yet no recognized solution. Research on OQDS is focused on finding strategies to control its spread or mitigate its symptoms. In this context, we investigated the feasibility of using low-temperature plasma and plasma-activated water to kill bacterial cells.

Experiments were conducted in vitro to test the biocidal effect of a Surface Dielectric Barrier Discharge plasma on bacteria. The results showed a high decontamination rate even for cells of XfDD embedded in biofilms grown on solid media. Application to trees requires protocols and tools that can reach the bacterium in the xylem vessels. Plasma Activated Water was tested as a biocidal agent that can move freely in the xylem network. Results in the liquid culture medium showed complete inactivation of XfDD cells and paved the way to test the strategy on infected plants.

Introduction

Xylella fastidiosa is a xylem-limited gamma proteobacterium whose pathogenic mechanism is based on the occlusion of the xylem vessels. The bacterium lives in biofilm communities embedded in an exopolysaccharide matrix from which clumps of cells are released to colonize infected plants systemically. Infection of new plants is mediated by insect vectors that feed in the xylem, ingest the bacterium and transfer it to new plants during successive feeding activities[1,2].

The "De Donno" strain of *Xylella fastidiosa* subspecies pauca haplotype ST53 was discovered in late 2013 in the Salento Peninsula (Apulia region) in olive trees that showed leaf burn, extensive desiccation of branches and plant death[3]. Soon after, this bacterial strain was found to be the causative agent of these symptoms, which were grouped under the name Olive Quick Decline Syndrome (OQDS)[3]. Although this strain infects the two main autochthonous olive varieties, Ogliarola salentina and Cellina di Nardò, it was also found in 595 other plant species, in several cases without showing symptoms[4].

The discovery of *X. fastidiosa* in this new environment and the infection mainly of olives has stimulated several research programs that have led to the description of the epidemiology of the infections in the epidemic area Salento Peninsula, the identification of *Philaenus spumarius* as an insect vector, the genomics of the bacterium and the response of olives to the infections[5].

The X. fastidiosa epidemic in southern Italy required the implementation of a series of phytosanitary measures enforced by European Authorities. These included intensive surveys to delineate the infected area and exclusion of the pathogen from non-infected areas in the Italian peninsula as well as in the

other Member States. The results of the surveillance program have confirmed that the infections are slowly spreading northwards into the southern part of Apulia. However, in addition to Italy, where a subspecies multiplex strain of X. fastidiosa has been found in Tuscany[6], other strains have been detected in France[7], Spain[8,9], Portugal[10] and recently in Israel[11], highlighting the serious threat that this quarantine bacterium poses to Mediterranean agriculture.

Bacterial cells are generally inactivated by physical and/or chemical sterilization. Physical methods such as heat and gamma radiation and chemical methods such as ethylene oxide are not suitable for curing *Xylella*-infected plants. Heat can cause irreversible damage to the plant, ethylene oxide is highly flammable and toxic, radiation processes require an isolated location and operator safety, and can cause DNA damage. These drawbacks are driving research for a novel, highly efficient sterilization process.

Among microbial inactivation strategies, non-thermal atmospheric pressure plasma has received increasing attention in biology, medicine[12–14] and the agricultural and food industries[15–17].

Surface treatments using this dry plasma technology offer an environmentally friendly alternative to conventional wet chemical methods for killing microorganisms. Extensive multidisciplinary research has been carried out over the last two decades, proving the validity of the application of plasma technology in the broad field of biology and medicine and antimicrobial clinical treatments against various pathogens.

Low- Temperature Plasma (LTP) offers numerous potential advantages over conventional methods, such as nontoxicity, low operating costs, short treatment time at low temperatures, a significant reduction in water consumption during the disinfection process, and applicability to a wide range of commodities[16,18–21].

In general, the effectiveness of LTP depends on the equipment design and system operating parameters, such as gas composition, flow rate, humidity, temperature, voltage, and frequency[22–24]. LTP in ambient air is an excellent source of electrons, positive and negative ions, free radicals, stable transformation products, excited atoms and molecules, and ultraviolet radiation (UV) with antimicrobial activity[25]. Most reactive species produced by plasma sources include electronically and vibrationally excited oxygen O_2 and nitrogen N_2; reactive oxygen species (ROS), such as atomic oxygen O, singlet oxygen $^1O_2$, superoxide anion O^-_2 and ozone O_3 and, in the presence of moisture, H_2O^+, OH^- anion, OH radical or H_2O_2[26]; reactive nitrogen species (RNS), such as atomic nitrogen N, nitrogen in the metastable state N2(A), nitrogen oxide NO. Target organisms are either directly exposed to plasma generated ROS and RNS together with UV light and/or pulsed electric field generated by the plasma. Generally, ROS species elicit an oxidative stress response leading to harmful oxidative cell damage[27,28] and consequently inactivation of microorganisms[29–39]. Hydroxyl radicals (OH) have a direct effect on the cell membranes of microorganisms, which are composed of a bilayer of glycerophospholipids and proteins and are susceptible to their attacks[40,41]. In addition to direct decontamination processes, plasma can also activate stress signalling cascades that enable the self-defence mechanism, especially in plants. RONS

produced in response to abiotic and biotic stresses act as signalling molecules[42] and induce the production of secondary metabolites that act as precursors of defence hormones and lead to the activation of defence genes[43–48] and the production of defence compounds[49,50]. In addition, ROS can ensure that the plant is in a redox state ready to respond rapidly to stress[51].

Recently, plasma-activated water (PAW) has attracted the attention of researchers. Many studies on PAW have shown that the main active substances of PAW are reactive oxygen species (ROS) and reactive nitrogen species (RNS)[52]. The main components of ROS include hydroxyl radicals, hydrogen peroxide, singlet oxygen, superoxide anions and ozone, while RNS mainly include nitrate, nitrite, peroxynitrite, nitric oxide radicals, ammonia and nitrogen[53]. The long-lived reactive species among them are hydrogen peroxide, nitrate, and nitrite. The physical and chemical properties of water such as conductivity, pH and redox potential are affected by plasma activation.

Research on PAW as a control strategy for diseases and pests is sporadic and experimental. Two areas of research are being pursued: one involves direct decontamination by PAW, the other involves activation of self-defence in the plant. It has been found that PAW reduces surface yeast[54], inhibits mycelial growth of *Fusarium graminearum*[55], and protects tomato plants from leaf spot disease caused by *Xanthomonas vesicatoria*[56]. Irrigation of tomato seedlings with PAW resulted in better growth morphology, oxidation, and expression of defence genes[12,57]. As for pests, control[22] PAW proved effective against *Planococcus citri*[58] and showed a high mortality rate under laboratory conditions. The mechanism leading to the killing of pathogenic bacteria on the plant surface[59] can be related to RNS and ROS, with ozone and peroxynitrite being the dominant factor in the sterilisation matrix[53,60–63]. Moreover, PAW may serve as a resistance inducer for plants by triggering their defences against pests and diseases and strengthening the plant pathogen defence pathway[64].

In the present manuscript, LTP and PAW were used to evaluate their antimicrobial activities against the strain "De Donno" of *Xylella fastidiosa* subspecies *pauca* haplotype ST53 (XfDD). Due to the difficulties of performing experiments in an unenclosed laboratory, we developed a portable device to generate plasma through a Surface Dielectric Barrier Discharge (SDBD) using ambient air with a measured relative humidity of approximately 40%. All treatments were performed in a laminar flow hood. We first investigate the feasibility of direct decontamination of bacteria by plasma by exposing the cell culture to the spatial afterglow of the SDBD for in vitro culture. The second step was to evaluate the effect of PAW in an XfDD suspension in a water-based solution. The basic idea of the proposed experiments is to find a possible strategy to achieve the decontamination of the surfaces exposed to the bacteria, such as tools or leaves, by using an atmospheric pressure plasma source and to apply the PAW as a novel tool to control the infection in plants, either by direct exposure of the pathogen to the RONS present in the PAW or by activating the self-defence mechanism of the plant.

Materials And Methods

Dielectric Barrier Discharge

The discharge system includes an SDBD reactor, gas feeding unit, discharge energization system, electrical and optical diagnostics, and sample holder suitable for inserting biological samples at a selected distance from the discharge surface. The SDBD reactor shown in panel (A) of Fig. 11, consists of a planar SDBD electrode system placed in a PVC chamber equipped with gas feed input/output ports and a high voltage (HV) interface.

The discharge was built starting from a glass petri dish, in which the electrodes were included (Fig. 11). The Ground electrode was equipped with an aluminium air-cooled dissipator to keep its temperature as close as possible to room temperature. The nickel electrode exposed to the discharge consists of 22 parallel stripes (0.2 mm wide, 10 mm long and separated by 1 mm). An aluminium induction electrode (55 mm x 55 mm) covers the opposite surface of the glass petri dish cover plate. The SDBD was powered by an AC power supply based on an Information Unlimited PVM500 - Plasma Power Generator. Applied AC HV waveform (19.6 kHz) was amplitude-modulated by a square-wave modulation waveform (f_M = 500 Hz) producing 19.6 kHz sine-wave T_{ON} and T_{OFF} periods with a fixed duty cycle D = $T_{ON}/(T_{ON}+T_{OFF})$ = 25% and a precise number of sine-wave bursts were selected through an external trigger realized using a TG 5011 Function Generator (TTi). We used Keysight InfiniiVision MSOX6004A Mixed-signal oscilloscope (bandwidth 1 GHz, up to 20 GS/s) to record the voltage–charge, voltage-current characteristics of the discharge. We used a Tektronix P6015A high voltage probe (1,000:1@1 MΩ, bandwidth 75 MHz) to monitor voltage waveforms, a Magnelab current transformer model CT-C1.0 (bandwidth 200Hz-500MHz) to measure the plasma current, and a voltage probe (100:1@10 MW, bandwidth 1 GHz) to measure the potential drop on a transferred charge measuring capacitor (C = 0.02 μF) inserted between the induction electrode and ground. The reactor was fed with humid air at a fixed flow rate of 7 slm. This reactor chamber allows the insertion of 50 mm in diameter standard Petri dishes (Fig. 11) next to the SDBD surface, with the top border approximately 3 mm far from the HV electrode. The same discharge setup was used to produce plasma-activated water (PAW).

The typical appearance of the HV electrode during the on-time is shown in Fig. 11B. Since we are dealing with quarantine bacteria the discharge was operated under a laminar flow hood (model Aura HZ48), in the authorized lab of the CNR IPSP in Bari (Fig. 11C).

Emission spectroscopy

To perform spectroscopic measurement a slightly modified version of the reactor was used to place UV grade quartz frontal windows allowing direct visual control of the discharge area and optical emission diagnostics. Optical emission spectroscopy was performed by collecting light from the SDBD plasma surface through a UV fused silica single-lens fibre optic bundle model LG-455-020-3 (3 meters, 190 to 1100 nm, with 19 200 μm fibres, 10 mm ferrule at slit end) equipped with UV grade quartz lenses system on the entrance slit of a monochromator. The imaged area collected light is limited by the entrance slit dimension and can reach a maximum dimension of 3 (l) × 5 (h) mm^2. The light is spectrally resolved by a

30 cm spectrometer (Acton Spectra Pro 2300), equipped with a multiple-grating turret with a 300/600/1200 grooves mm^{-1}, blazed at 300 nm, and covering the ranges 200–1400 nm. The spectrum is acquired with a Princeton Instruments PI-MAX4 1024i CCD camera equipped with a 1024x1024 pixel sensor (size 12.8 um, active area 13.1 × 13.1 mm^2). One CCD image of a spectrum covers a range of approximately 144/65/30 nm respectively for the three different gratings. The intensities of the emission spectra acquired by the ICCD detector were spectrally and intensities were corrected utilizing Halogen (oriel) and calibration lamps (oriel). The spectra were used to evaluate rotational temperatures and vibrational distributions. Spectra were simulated to infer rotational temperature information using the freely available spectroscopic tool Massive OES [65–67].

PAW characterization

Spectrophotometric measurements

An aliquot of 3 ml of ultrapure water was treated at different times (5, 15 and 30 min) with Surface Dielectric Barrier Discharge plasma (SDBD) to evaluate the change in the content of nitrates and nitrites, H□O□, pH value and the changes in the electric properties. The treatment times were progressively increased to study changes in the water compared with the untreated sample. Three replicates of measurement were set up and the mean value was recorded. The pH value was measured with the pH meter pH50 Lab (XS Instruments, Carpi MO - Italy) at room temperature.

The content in nitrates and nitrites was measured with a UV-Visible Spectrophotometers Thermo Scientific™ Evolution™ 201 (Thermo Fisher Scientific Inc., Madison WI, USA) following the protocol indicated in the Nitrate and Nitrite Test Spectroquant® (Merck KGaA, Darmstadt, Germany). The Nitrite content was evaluated at the absorbance value of 525 nm with the dilution of 1:5 of the water sample, following the kit procedure parameters, whereas the nitrate content was evaluated at 340 nm without dilution of the water sample. The peroxide (H□O□) content in the analysed water was measured with the Peroxide Test MQuant® (Merck KGaA).

Measures were repeated 24 h after the activation of water, in samples treated and kept at 4°C, to evaluate changes in the content during the time.

Electrical Impedance (EIS) and Broadband Dielectric Spectroscopy (BDS)

We performed EIS measurements on untreated deionized water (DIW) and plasma-activated water (PAW) at two different plasma treatment times (5 min and 15 min) using a two-probe cell built on 4 ml glass vials. The electrical feedthroughs of the cell consisted of two glass capillary tubes inserted and sealed through a hole in the top of the vial stopper. The capillary tubes allowed the insertion of two gold plated needles, spaced L = 2 mm apart, into the interior of the vial to make electrical contact with the internal water. The needles were then connected to the measurement apparatus via a BNC cable. Impedance (Zvsf) spectra were recorded using a NOVOCONTROL Impedance Analyzer. The AC voltage signal (V_{AC})

was fixed at 30 mV and the frequency range was between 0.1Hz and 1.0 MHz. It took about three minutes to record one spectrum.

Since the magnitude of the impedance depends on the volume and density of the test sample, we perform the measurements with the same amount (3ml) of plasma-activated (PAW) and untreated deionized water (DIW) to obtain the same comparison. We also repeat the measurements on 15 min treated PAW samples after 24 hours to assess the ageing effect due to the instability of the ion concentration.

The instrument software provided the spectra of the real (ReZ) and imaginary (-ImZ) parts of the impedance and the corresponding phase φ, where φ = arctan (ImZ/ReZ)). We plot the impedance outputs using the Nyquist plots (NPs) i.e. –ImZ *vs.* ReZ. We then fit the impedance of a suitable electrical circuit using the free downloadable software EIS Analyzer [80]. Generally, the NP region on the right (left)side corresponds to the low (high) frequency response. In general, the circuit consists of a suitable combination of resistor R, capacitance C, Constant Phase Elements, Z_{CPE} and a Warburg Element, Z_W. The Z_{CPE} is a non-intuitive impedance expressed by[81]:

$$Z_{CPE} = \frac{1}{Q_0(j\omega)^n};$$

1

where Q_o^{-1} is the impedance magnitude modulated by the n value and it is introduced to simulate a non-perfect capacitive response

In (1) the Q_o^{-1} term is expressed in $\Omega^{1-n}F^n$ with $0 < n < 1$; therefore, when n is close to 0 the impedance behaves like a resistor whereas when is close to 1 it behaves like a pure capacitance. The Warburg element Z_W is the equivalent circuit element assigned to the diffusion process and it is expressed as:

$$Z_W = \frac{A_W}{\sqrt{\omega}} + \frac{A_W}{j\sqrt{\omega}};$$

2

i.e. via a constant phase element where the n value is 0.5. In the complex plane, the diffusion element is recognized as a straight line in the NP with a slope of 45° to the real axis.

To gain better evidence on the ionic concentration and conductivity useful for the understanding of the PAW redox activity level, we represent the impedance data via the dielectric loss factor tanδ expressed via the ratio between the real ε' and imaginary ε" part of permittivity i.e.[82]:

$$\epsilon' = \frac{-ImZ}{2\pi f C_0 |Z|^2}; \epsilon'' = \frac{ReZ}{2\pi f C_0 |Z|^2}$$

3
via

$$tan\delta = \frac{\epsilon''}{\epsilon'}$$

4
The dielectric loss relates directly to the AC conductivity and then to the PAW pro-oxidant environment feature since:

$$\sigma = \omega\epsilon_0\epsilon'' = \omega\epsilon_0\epsilon' tan\delta = \sigma_{DC} + A\omega^n \quad (5)$$

The expr. 5 shows that the AC conductivity is composed of a frequency-independent part associated with the ionic DC conductivity and a component that depends on the frequency of the voltage signal. In general, the σ vs ω is characterized by the region attributed to electrode polarization effects in the low-frequency range followed by a plateau in the mid-frequency range (i.e., after the tanδ peak where the σ not depends on the signal frequency and is attributed to the ionic DC conductivity σ_{DC} and then by a region attributed to ionic hopping, which generally follows Johnsher's power law with $0 < n < 1$ [83].

Following the Macdonald-Truckam model [84] the peak value of the loss factor and the corresponding angular frequency relates to ions diffusivity D:

$$D = \frac{\omega_{max} L^2}{32\left(tan\delta_{max}\right)^3}$$

6
Since $\sigma_{DC} = n\ q\ \mu$ (n the ionic concentration, q the elemental charge and μ the mobility of the ions) and the diffusivity $D = k_B T/q\mu$ with k_B the Boltzman constant and T the temperature, it follows that the ionic concentration can be determined via:

$$n = \frac{\sigma_{DC}}{D}\frac{k_B T}{q^2} \quad (7)$$

Xylella fastidiosa growth conditions and plasma treatments

X. fastidiosa subsp. *pauca* strain "De Donno" ST53 was used in this study[85]. Bacteria were cultured on BCYE agar plates for 15–20 days at 28°C.

Plasma treatments were carried out on bacteria that directly grow on solid (agar amended) media or after suspension in PAW.

Treatment on agar surface-grown bacteria

XfDD was currently grown on BCYE agar plates at 28°C and the inoculum was regularly renewed every 7 days on new plates. Cells were collected from the agar surface with a sterile loop, resuspended in 1x PBS buffer and adjusted, before plating, to a final concentration of $4x10^8$ CFU ml^{-1} (OD600 0.5).

Trials were carried out using different bacteria concentrations, from 10^7 to 10^3 CFU ml^{-1} after resuspending cells scraped from an agar plate in PBS. Forty microliters of bacteria were plated by spreading on the agar surface using a sterile loop. Preliminary tests were carried out to find the best conditions of treatments, particularly referring to the initial bacteria concentration, the pre-culture of the bacteria before plasma exposure and duration of the exposure. To this aim, bacteria were pre-cultured for 1 and 5 days before being exposed to LTP which was discharged for 10, 100 and 200 s. LTP untreated cells grown in the same conditions were used as control. The plates were incubated at 28°C for up to 30 days and the antibacterial activity was assessed using the viable plate count method [86]. The number of CFU ml^{-1} in the control plate was determined by multiplying the number of colonies on a dilution plate by the corresponding dilution factor. Only plates (or replicate plates from the same dilution) with 30–300 colonies were counted[87].

In addition, the cumulative effect of the LTP was evaluated by applying the SDBD plasma a) one time a day for 1 week, and b) one time a week for 3 weeks at the maximum exposure time of 200 s. In these trials XfDD was pre-cultured for 1 and 7 days in a) and b) respectively, before being exposed to LTP treatment.

Plates were preliminarily treated with LTP for an exposure time of 200 s and successively inoculated with XfDD to evaluate if the plasma treatment could alter the chemical/physical properties of the BCYE agar substrate and therefore inhibit the growth of the bacterium.

Each assay was performed in triplicate, and each experiment was repeated at least two times.

Treatment cells with Plasma Activated Water (PAW)

Deionized water (DIW) (18.2 MΩ·cm at STP) was obtained from a Millipore Direct-Q 3UV system. 500 ml of DIW were stored in a container in an ambient atmosphere for one day. This procedure enabled the concentrations of gases dissolved within the DIW to equilibrate with the air, which ensured constant concentrations of gases between experiments. Three ml of DIW were transferred to a 50-mm-diameter petri dish inserted in the SDBD discharge chamber and treated for 15 min. The free surface of the water was approximately 3 mm far from the SDBD HV electrode. The PAW was then immediately used to resuspend bacteria to a final concentration of 10^7 CFU ml^{-1}. The LIVE/DEAD ®BacLight™ (Molecular Probes) viability kit was used to assess the viability of bacteria cells treated with PAW. The kit contains a vial of microsphere suspension, and two nucleic acid dyes SYTO 9 and propidium iodide (PI) that allow distinguishing live cells with intact plasma membranes (green) from dead bacteria with compromised membranes (red). Bacteria suspensions were incubated at room temperature for 15 min in the dark in a solution of equal volumes of the two stains. Photomicrographs were taken on a Nikon E800 microscope

using a fluorescein isothiocyanate (480/30 excitation filter, DM505 dichroic mirror, 535/40 emission filter) and tetramethylrhodamine isocyanate (546/10 excitation filter, DM575 dichroic mirror, 590 emission filter) fluorescence filter sets.

Results

Plasma Current Voltage and Emission Spectroscopy

The SDBD was operated in humid ambient air (25°C, 40% RH) at atmospheric pressure. The applied AC voltage (20.6 kVpp (peak-to-peak), see Fig. 1) consisted of repetive burst (repetition rate 500Hz), each consisting of nine AC cycles (f_{AC} = 19.6 kHz) with a repetition rate of 500 Hz (duty cycle of 0.25). In this way we obtained a homogeneous distribution of microdischarges. The actual discharge ON-time is shorter than the duration of the AC cycles. We can estimate an effective duty cicle of the order of 0.1 of the nominal one[53]. This ensures that biological samples are not exposed to excessively damaging temperatures. Typical voltage, current, and charge characteristics are shown in Fig. 1A-C, along with the typical Lissajous figure showing the charge voltage characteristic (Fig. 1D) used to determine the discharge energy. The estimated energy per burst is about 4.5 mJ, i.e. an average power of 2.25 W, with an energy density of 3.8 10^{-2} Wh L^{-1}. The air-SDBD operated in ozone mode, and we can expect a concentration on the order of 200–300 ppm, well above the concentration of nitrogen oxide products[13,53].

Figure 2 shows low-resolution emission spectra of filamentary SDBD operating in humid air, and reveals strong bands of the second positive system (SPS) ($C^3\Pi_u \rightarrow B^3\Pi_g$) of N_2 and the first negative system (FNS) ($B^2\Sigma_u^+ \rightarrow X^2\Sigma_g^+$) of N_2^+ in the UV spectral region. In the Vis-NIR region, we observed characteristic sequences of bands of the first positive system (FPS) ($B^3\Pi_g \rightarrow A^3\Sigma_u^+$) of N_2. The emission line for atomic oxygen was observed at 777 nm, indicating the production of atomic oxygen during the plasma phase. The partially resolved structures of SPS (0,0) shown in Fig. 3 were analysed using the Massive OESspectroscopy tool[65–67]. The SPS (0,0) band can be fitted for a specific instrumental function by setting the rotational temperature to 350 ± 25 K. This temperature represents the gas temperature during the discharge on phase near the dielectric surface, where plasma is confined in SDBDs. Thus, it does not represent the temperature of the gas in direct contact with the treated substrate. Also, considering that the gas flows at 7 slm, which gives a residence time in the discharge volume of 64 ms, we can rule out heat accumulation within the gap.

Figure 3 shows the experimental SPS(0,0) band profile along with three synthetic profiles (simulated for rotational temperatures of 300, 350 and 400 K) on a logarithmic scale to demonstrate the sensitivity of the band tail of the band (formed by the overlap of the R_1, R_2 and R_3 branches) to the rotational temperature of the $C^3\Pi_u$ state.

Figure 4, shows the emission formed by the Δv = -3 and − 2 sequences of the SPS and by the Δv = 0 sequences of the FNS. From Fig. 4, the ratio between FNS(0,0) and SPS(0,3) is equal to 0.6 ± 0.02. From

the FNS/SPS calibration curves[66] we can estimate that the averaged reduced electric field E/N is more than 900 Td.

Figure 5 shows the characteristics of the vibrational distributions of $N_2(C^3\Pi_u)$ obtained from the time- and space-averaged spectra shown in Fig. 4, together with three Boltzman vibrational distribution functions (VDFs) corresponding to the vibrational temperature of 2500K, 2750K and 3000K. We can conclude that the experimental VDF is characterized by a clear non-Boltzman behaviour.

PAW Characterization

Chemical properties of PAW

The content of nitrate and nitrite (mg/L) of PAW was measured and their stability in water after plasma activation was evaluated. The mean value of nitrate (25.7 mg/L) in water sample exposed to 15 min of SDBD plasma activation was kept almost constant (22.8 mg/L), while the nitrite content was drastically reduced (started from 26.9 mg/L to 16.4 mg/L) after 24 h storage at 4°C from the activation. The pH value increased from an initial mean value of 3.4 to 4.3. The level of hydrogen peroxide measured through a colourimetric test decreased from 5–10 mg/L to 2–5 mg/L.

Electrical Impedance (EIS) and Broadband Dielectric Spectroscopy (BDS) results.

The results of EIS and BDS allowed rapid monitoring of PAW properties. The effect of plasma treatment was evaluated by ion density n and estimation of ionic conductivity. In this way, it was possible to predict the effectiveness of the PAW treatment on the XfDD.

In Fig. 6, we show the comparison between NPs (Fig. 6A) as calculated from the impedance of untreated deionized water (DIW) and PAW. The latter refers to two representative plasma treatment times of 5 min and 15 min, which are of interest for this work. The inset shows the magnified view of the region in the high-frequency region.

It is worth noting that there are significant differences between the NPs associated with the DIW (black curves) and the NPs from PAW.

We obtained the best fit with the circuit (see Fig. 6B and Table 1) consisting of the series of two components, namely the parallel $R_1//Z_{CPE}$ related to the response in the low-frequency region and specifically in the $f < 100$ Hz region, and a modified Randle circuit related to the $f > 100$ Hz frequency region.

Table 1
EIS parameters extracted by the best fit of the experimental Nyquist plots in Fig. 7A with that one of the equivalent circuits represented in Fig. 7B.

ITEMτ	DIW	PAW 5min	PAW 15min	PAW 15 min ag
$R_1(\Omega)$	10956	$1.95x10^5$	$1.34x10^5$	$3.84x10^5$
Z_{CPE}	$6.7x10^{-10}$	$9.10x10^{-6}$	$8.10x10^{-6}$	$5.18x10^6$
$(\Omega^{1-n}F^n)$	0.95	0.88	0.96	0.84
n				
C_{DL}	$2.9x10^{-11}$	$2.70x10^{-11}$	$2.72x10^{-11}$	$2.88x10^{-11}$
$Z_W(\Omega\ s^{-0.5})$	$1.4x10^5$	25811	41011	19989
$R_{ct}(\Omega)$	$4.1x10^5$	15151	5414	6772

The $R_1//Z_{CPE}$ component is assigned to the interaction of the solution at the interface with the electrodes (electrode polarization, EP effect), while the Randle circuit corresponds to the electrochemical processes within the solution[69]. Following the theory of Bard and Faulkner, the processes involve redox reactions whose effectiveness can be evaluated by the value of the charge transfer resistance R_{ct}, which is also an index of the magnitude of the charge transfer current I_{ct} ($I_{ct} \propto R_{ct}^{-1}$), and then for the ions and free electrons involved in the redox process[70].

It is noteworthy that the impedance $Z_R = R_{ct} + Z_w$ as a function of the treatment time τ is related to the concentration of ionic species determined by the optical absorption methods ρ_{abs} (Fig. 6B) and represents a fingerprint of the production and total evolution of NO_3^- and NO_2^- radicals and hydrogen peroxide concentration with treatment time. On the one hand, the decrease of ion diffusivity underlined by the increase of Z_W ($Z_W \propto D^{-1}$) is due to the increase of ion concentration; on the other hand, the R_{ct} shows the increase of charge transfer current ($I_{ct} \propto R_{ct}^{-1}$) and then the presence of free redox electrons and underlines the onset of a dominant oxidant environment.

We gain further information on ionic diffusivity D and species concentration n determined via the analysis of dielectric permittivity returned from BDS data. In Fig. 7 we summarize the AC conductivity (left axis) (σ(ω) vs ω) and the loss factors tan δ frequency dispersion (tan δ vs ω) (right axis) together with the values of the ionic diffusivity, D, and concentration, n, calculated with expr. 5,6,7. Interestingly, the value of the continuous part of the AC conductivity σ_{DC} evidenced by the plateau starting at around f > 100Hz (Fig. 7A) is increasing with the treatment time. Moreover, the σ_{DC} PAW response is not much

affected by an ageing time of 24 h (15 min ag) thus confirming the stability in a time of the oxidant environment.

We also compare the tanδ in PAW with that one of the well-known chemical reactions in a solution H_2O_2 + HNO_3 (1:1) progressively diluted in DIW (data not shown). This is because in both cases the reaction products are the same (i.e., NO_3^-, NO_2^- and H_2O_2). Moreover, the dilution in DIW allowed the use of the known ionic charges' concentration of the chemical reaction to calibrate those observed in PAW vs treatment time (data not shown). The cross-checks of the tanδ of the chemical reaction and PAW spectra allowed us to conclude that BDS results on PAW are consistent with those of the chemical reaction either because of the similar spectral features or the concentration of the ionic charge whose value was found furthermore in agreement with those derived from optical methods.

We can observe (Fig. 7A) that the position tan δ peak of PAW shifts to a higher frequency than that of DIW, which is associated with a decrease in peak intensity compared to treatment time. In addition, the 15min ag PAW item shows a slight increase in tan δ peak intensity with no change in frequency and similar values of σ_{DC}. Consequently, we observed a decrease in the concentration of ionic charges and a corresponding increase in the diffusivity D. This behaviour could be related to the decomposition of hydrogen peroxide and nitrogen peroxyacids[52]. However, the results of EIS and BDS show that the pro-oxidant environment can still be effective after 24 hours.

Although we can only quantify the total concentration of ionic species at this time, we found a linear correlation between the ion diffusivity D or the total concentration of PAW ionic species n and the total concentration ρ_{abs} (A) measured by chemical methods.

XfDD growth conditions and plasma treatments

Treatment on agar surface-grown bacteria

Preliminary investigations showed that the plasma pre-treatment of the agar plates did not alter the growth of XfDD cells (data not showed).

When bacteria (10^7 CFU ml^{-1}) were plated out on Buffered Charcoal Yeast Extract (BCYE) agar and exposed to SDBD for 200 s, complete inhibition of cell growth was observed, whereas after 100 s and 10 s of exposure (Fig. 8) there was less pronounced but time-dependent inhibition.

Since it is difficult to quantify the effect of plasma treatment by counting colonies at a concentration of 10^7 CFU ml^{-1} (Fig. 9), decimal dilutions from 10^5 to 10^3 CFU ml^{-1} of XfDD inoculum were applied to the BCYE agar plates in subsequent experiments (trials). Final SDBD plasma treatment conditions were therefore performed on cells grown 1–5 days after seeding, with a maximum exposure time of 200 s.

Table 2 shows the results for different three dilutions (10^3, 10^4, 10^5) for untreated and 200 s treated plates pre-cultured for one or five days before LTP exposure. The treatment was effective and complete

removed of all bacteria by plasma, at both 1 and 5 days.

Table 2
Results of the experiment performed on agar surface grown XfDD. Treatment time was fixed at 200 s following the finding of the previous experiment. We performed experiments in triplicate for a total of 9 dishes for each experiment. The experiments were conducted on plates just at T0 = 0 and T5 = 5 days after XfDD seeding.

Concentration	T_{ime}	N of replicas	11 days CFU ml^{-1}	13 days CFU ml^{-1}
10^5	untreated	3	$3.8x10^8$	$9.8x10^8$
10^4		3	$4x10^5$	$2.1x10^7$
10^3		3	0	$2x10^5$
10^5	T0	3	0	0
10^4		3	0	0
10^3		3	0	0
10^5	T5	3	0	0
10^4		3	0	0
10^3		3	0	0

When plasma interacts with a surface, its energy (in the form of ions, RONS, and UV radiation) is deposited in the exposed matrix. Multiple exposures result in a cumulative effect of absorbed doses leading to progressive destruction of the microorganism. To evaluate the effect of the LTP dose-effect, we performed a repeated plasma treatment of 200 s with two different frequencies: 1 treatment per day for a period of 10 days (Trial a) and once per week for a period of three weeks (Trial b).

The results of these experiments are given in Table 3 and show that in Trial a) a strong effect of cumulative dose was observed, since at the lower concentration (10^3 CFU ml^{-1}) the bacteria were completely killed by the multiple exposures, resulting in a reduction of at least log 5, while at higher CFU the reduction reached at least a log 2 value. In Trial b), cells were counted 20 days after plating. The concentration-dependent effect was less pronounced. Treatment resulted in a reduction of at least log 1 for the lower concentrations (10^3 CFU ml^{-1}, 10^4 CFU ml^{-1}), whereas at 10^5 CFU ml^{-1} counting was not possible for the untreated sample, making it difficult to estimate the reduction.

Table 3
Results of the dose dependence experiment performed on BYCE agar surface grown XfDD

Treatment frequency	Initial Concentration (CFU mL^{-1})	CFU ml^{-1} at day			
		11	13	15	20
untreated	10^5	$1,1x10^9$	$1,9x10^9$		not count
	10^4	$1,2x10^6$	$6,3x10^7$		$7,5x10^7$
	10^3	0	$6x10^5$		$2,8x10^6$
Trial a) 1 per day	10^5	$3.3x10^6$	$4.1x10^6$		
	10^4	$8.3x10^4$	$3.3x10^5$		
	10^3	0			
Trial b) 1 per week	10^5			$3.5X10^7$	$1.6x10^8$
	10^4			$3.3x10^5$	$1.7x10^6$
	10^3			0	$1x10^5$

Treatment of cells with Plasma Activated Water (PAW)

To test the efficacy of plasma treatment and its potential for use in vivo, bacteria were suspended in PAW previously treated in the SDBD discharge chamber for 15 minutes. To decipher the exact mode of action of the plasma treatment, its effect on XfDD was monitored using viability assays with fluorescence live/dead staining.

Fluorescent probes were used to assess cell membrane integrity and XfDD viability after incubation in PAW. The untreated control cells were almost all stained green with SYTO 9, indicating that they were viable. A small number of cells were stained red with propidium iodide (PI), indicating that they were probably dead (Fig. 10A). The number of cells stained red with PI increased dramatically after treatment with PAW, while cells stained with SYTO 9 decreased as expected and only a few fluorescent cells were visible after treatment (Fig. 10 (B)). This indicates that the integrity of the cell membrane of the bacteria was damaged by the treatment, affecting their viability.

Discussion And Conclusions

In the present study, we investigated the effects of LTP application on XfDD inactivation. Our results showed that an exposure time of 200 seconds was sufficient to reduce the number of bacterial cells to an undetectable level, proving that LTP is a cost-effective and environmentally friendly alternative to

disinfection by chemical and physical means. Furthermore, we demonstrated that the LTP effect is cumulative, opening the possibility of multiple exposure runs.

The plasma chemistry is highly dependent on the composition of the feed gas, the configuration of the system and the operating conditions. Air plasma is a rather complex environment in terms of chemical composition (RONS) and light emission (from UV to mid-range IR, mainly due to molecular nitrogen systems). Using the optical emission spectrum (OES) recorded at about 3 mm from the SDBD surface, we observed weak emissions from the Nitric Oxide gamma band covering the UV-C region (200–280 nm), from OH (mainly in the presence of water) and N2 SPS in the UV-B region (280–315 nm). Thus, direct photooxidation of the protein coat is not considered to be the dominant inactivation process. The strongest emission was observed in the UV-A region (315–400 nm), due to the SPS, FNS band systems of N2. Although we cannot exclude UV-A-mediated bacterial disinfection[71,72], this cannot be the main process leading to cell death due to the reported exposure time and energy density.

From the SPS (0,0) emission and comparison with the corresponding simulation spectra, we can also rule out heat as a possible mechanism for the disinfection of the samples.

From the emission spectroscopy in the mid- IR, we observed also the presence of atomic oxygen at 777 nm could not be detected. The discharge currently operates in ozone mode, since ozone is the main post-discharge product along with NOx. Thus, the main disinfection mechanism could be due to oxidative pressure by the reactive oxygen and nitrogen species (RONS), which are produced by plasma and are toxic to bacterial pathogens at high concentrations. These RONS oxidize proteins, lipids and nucleic acids and lead to the destruction of the pathogen. They also cause epigenetic regulation that could abrogate bacterial pathogenicity[73]. The efficacy of the treatment fixed at 200 s makes disinfection a rather rapid process in the case of planktonic cells. Moreover, pretreatment of the cell culture medium with plasma does not result in sufficient changes in substrate chemistry leading to apoptosis of the cells. The presence of biofilm in the cell culture makes it difficult to treat once with the selected fixed time. This can be overcome by increasing the plasma dose. Since we wanted to keep the plasma parameters constant, we decided to increase the plasma dose by repeating the treatment with a different frequency. This guarantees that we keep the temperature of the plasma phase close to room temperature and preserve the electrode from possible failure.

In this case, the best results were obtained with a repeated daily treatment for 1 week, which stopped cell growth and resulted in at least a log-2 reduction in bacterial colonies.

We could conclude that the main mechanism of the process is related to the RONS generated by the discharge device. However, for the practical use of LTP, the bacteria must be treated in their natural habitat, the xylem vessels of the plant. To meet these biological requirements, we investigated the use of PAW, to inactivate the bacterium, as this is a valid approach to control XfDD in plants.

PAW has attracted much attention from researchers in the last decade due to its non-thermal and non-toxic mode of action, which is mainly due to the reactive species that can react with the bacterial

structural components and later with organelles, proteins and nucleic acid, leading to cell death[74] It has been shown that the effect of the active species produced on PAW on bacteria depends on the bacterial species: In general, gram-negative bacteria were found to be more sensitive to PAW than gram-positive bacteria due to significant differences in cell wall structures, physiological state, and ultimately planktonic or biofilm status[75]. The PAW contains RNS and ROS, which can enter bacterial cells through the immediate pores in the active transport cell membrane. The RNS and ROS can oxidize DNA, proteins, and lipids in the cell, breaking DNA, degrading proteins, and inducing lipid peroxidation thereby causing the contents to flow out of the bacteria and die[59], with ozone and peroxynitrite being the dominant species in the sterilization process[53,60–62]. Many researchers also speculate that acidity and active compounds are related in PAW. In an acidic environment, the RNS and ROS will react with the lipids and carbohydrates of the DNA proteins in the cells, lowering the pH of the cells and causing physiological dysfunction and cell death63. In addition, the effects of PAW on biofilms have also been explored[75–78]. The importance of biochemically reactive species formed in PAW for the destruction and degradation of the biofilm matrix and the release of resident microbial cells have been highlighted[79].

In our experiment, we used freshly prepared PAW obtained by activation of sterile water by SBDB in air. Assuming that the activity of PAW in terms of sterilisation properties is due to the presence of peroxynitrous acid (which requires nitrite, peroxide and acidic conditions)[52], freshly prepared PAW by cold plasma processes should be the most efficient means. Chemical analysis of freshly prepared PAW at a treatment time of 15 minutes showed the presence of nitrite, nitrate, and hydrogen peroxide. Nevertheless, the PAW proved to be sufficiently stable for 1 day when stored in an opaque container at a temperature of 4°C. The EIS and BDS were used as rapid and non-destructive techniques to monitor the redox activity of PAW as a function of plasma treatment time. This is evidenced by the behaviour of the charge transfer resistance and DC conductivity, both of which are markers of a pro-oxidant environment. In our case, the latter activity is particularly pronounced at the 15-min treatment time PAW as can be deduced from the values of both electrical parameters. Interestingly, we found a correlation between the total ionic charge concentration and diffusivity determined by EIS and DBS and the total ionic concentration determined by optical methods. The higher nitrate, nitrite and peroxide content of the freshly produced PAW was indicative of the best treatment efficacy in this case. Nevertheless, the aged PAW redox environment is an indication that the treatment could be effective even after 24 hours.

Our results showed that PAW has excellent antimicrobial potential to inactivate X. fastidiosa cells. Just 15 minutes of treatment is sufficient to destroy XfDD cells in in vitro experiments. This is an important step towards the development of plasma-assisted strategies to inhibit the growth or kill XfDD in the xylem vessels of plants and to apply an environmentally safe strategy to control this pathogen, which will be the progress of the present work.

Declarations

Acknowledgement

This work was partially funded by by Italian Ministero dello Sviluppo Economico [Project PROTECTION ; Programma Operativo Nazionale «Imprese e Competitività» 2014-2020 FESR ; grant number Protection F/050421/01-03/X32]. P.F.A. and M.A. acknowledge the Potenziamento Strutturale PONa3_00369 “Laboratorio per lo Sviluppo Integrato delle Scienze e delle TEcnologie dei Materiali Avanzati e per dispositivi innovativi (SISTEMA)” dell’Università degli Studi di Bari “A. Moro”.

Author Contributions statement

P.F.A. Designed and conducted the experiments, wrote the manuscript, S.Z. conducted the experiment(s), wrote part of the manuscript, M.A. conducted the experiment(s), wrote part of the manuscript, P.R.R. conducted the experiment(s), wrote part of the manuscript; M.S. critical revision and manuscript writing; D.B.; critical revision and manuscript writing; A.D. lab work and manuscript writing; P.S. experimental plan, critical revision and manuscript writing

Corresponding Authors

Correspondence to Paolo F. Ambrico (paolofrancesco.ambrico@cnr.it) or Pasquale Saldarelli (pasquale.saldarelli@ipsp.cnr.it)

Competing interests

The authors declare no competing financial interests.

References

1. Redak, R. A. *et al.* The Biology of Xylem Fluid-Feeding Insect Vectors Of Xylella fastidiosa and Their Relation to Disease Epidemiology. *Annual Review of Entomology*, https://doi.org/10.1146/annurev.ento.49.061802.123403 (2004).
2. Schaad, N. W., Postnikova, E., Lacy, G., Fatmi, M. & Chang, C. J. Xylella fastidiosa subspecies: X. fastidiosa subsp piercei, subsp. nov., X. fastidiosa subsp. multiplex subsp. nov., and X. fastidiosa subsp. pauca subsp. nov. *Syst. Appl. Microbiol*, **27**, 290–300 (2004).
3. Saponari, M., Giampetruzzi, A., Loconsole, G., Boscia, D. & Saldarelli, P. Xylella fastidiosa in Olive in Apulia: Where We Stand. *Phytopathology*, **109**, 175–186 (2019).
4. Update of the Xylella spp. host plant database – systematic literature search up to 30 June 2019.*EFSA J.***18**, (2020).
5. Saponari, M. *et al.* Isolation and pathogenicity of Xylella fastidiosa associated to the olive quick decline syndrome in southern Italy. *Sci. Rep*, **7**, 1–13 (2017).

6. Marchi, G. *et al.* First detection of Xylella fastidiosa subsp. multiplex DNA in Tuscany (Italy). Phytopathologia Mediterranea(2018). doi:10.14601/Phytopathol_Mediterr-24454
7. Soubeyrand, S. *et al.* Inferring pathogen dynamics from temporal count data: the emergence of Xylella fastidiosa in France is probably not recent. *New Phytol*, https://doi.org/10.1111/nph.15177 (2018).
8. Olmo, D. *et al.* Landscape Epidemiology of Xylella fastidiosa in the Balearic Islands. *Agronomy*, https://doi.org/10.3390/agronomy11030473 (2021).
9. Xylella fastidiosa. *Ministerio de Agricultura, Pesca y Alimentación* Available at: https://www.mapa.gob.es/es/agricultura/temas/sanidad-vegetal/organismos-nocivos/xylella-fastidiosa/.
10. Delbianco, A., Gibin, D., Pasinato, L. & Morelli, M. Update of the Xylella spp. host plant database – systematic literature search up to 31 December 2020.*EFSA J.* **19**, (2021).
11. First report of Xylella fastidiosa in Israel 2019/121. *EPPO Reporting Service* (2019). Available at: https://gd.eppo.int/reporting/article-6551.
12. Kaushik, N. K. *et al.* Biological and medical applications of plasma-activated media, water and solutions. *Biol. Chem*, **400**, 39–62 (2018).
13. Martines, E. Special issue 'plasma technology for biomedical applications'.*Appl. Sci.***10**, (2020).
14. Choi, E. H., Uhm, H. S. & Kaushik, N. K. Plasma bioscience and its application to medicine.*AAPPS Bull.***31**, (2021).
15. Puač, N., Gherardi, M. & Shiratani, M. Plasma agriculture: A rapidly emerging field. *Plasma Process. Polym*, **15**, 1700174 (2018).
16. Ambrico, P. F. *et al.* Surface Dielectric Barrier Discharge plasma: a suitable measure against fungal plant pathogens. *Sci. Rep*, **10**, 1–17 (2020).
17. Misra, N. N., Tiwari, B. K., Raghavarao, K. S. M. S. & Cullen, P. J. Nonthermal Plasma Inactivation of Food-Borne Pathogens. *Food Eng. Rev*, **3**, 159–170 (2011).
18. Hähnel, M., Von Woedtke, T. & Weltmann, K. D. Influence of the air humidity on the reduction of Bacillus spores in a defined environment at atmospheric pressure using a dielectric barrier surface discharge. *Plasma Process. Polym*, **7**, 244–249 (2010).
19. Ambrico, P. F. *et al.* Reduction of microbial contamination and improvement of germination of sweet basil (Ocimum basilicum L.) seeds via surface dielectric barrier discharge. *J. Phys. D. Appl. Phys*, **50**, 305401 (2017).
20. Guo, J., Huang, K. & Wang, J. Bactericidal effect of various non-thermal plasma agents and the influence of experimental conditions in microbial inactivation: A review., **50**, 482–490 (2015).
21. Keener, K. M. M. & Misra, N. N. N. *Future of Cold Plasma in Food Processing. Cold Plasma in Food and Agriculture: Fundamentals and Applications* (Elsevier Inc., 2016). doi:10.1016/B978-0-12-801365-6.00014-7

22. Dobrynin, D., Fridman, G., Friedman, G. & Fridman, A. Physical and biological mechanisms of direct plasma interaction with living tissue. *New J. Phys*, **11**, 115020 (2009).
23. Wan, J., Coventry, J., Swiergon, P., Sanguansri, P. & Versteeg, C. Advances in innovative processing technologies for microbial inactivation and enhancement of food safety - pulsed electric field and low-temperature plasma. *Trends Food Sci. Technol*, **20**, 414–424 (2009).
24. Ehlbeck, J. *et al.* Low temperature atmospheric pressure plasma sources for microbial decontamination. *J. Phys. D. Appl. Phys*, **44**, 013002 (2010).
25. Kvam, E., Davis, B., Mondello, F. & Garner, A. L. Nonthermal Atmospheric Plasma Rapidly Disinfects Multidrug-Resistant Microbes by Inducing Cell Surface Damage. *Antimicrob. Agents Chemother*, **56**, 2028–2036 (2012).
26. Scholtz, V., Pazlarova, J., Souskova, H., Khun, J. & Julak, J. Nonthermal plasma — A tool for decontamination and disinfection. *Biotechnol. Adv*, **33**, 1108–1119 (2015).
27. Imlay, J. A. The molecular mechanisms and physiological consequences of oxidative stress: lessons from a model bacterium. *Nat. Rev. Microbiol*, **11**, 443–454 (2013).
28. Joshi, S. G. *et al.* Nonthermal Dielectric-Barrier Discharge Plasma-Induced Inactivation Involves Oxidative DNA Damage and Membrane Lipid Peroxidation in Escherichia coli. *Antimicrob. Agents Chemother*, **55**, 1053–1062 (2011).
29. Fang, F. C. Antimicrobial reactive oxygen and nitrogen species: Concepts and controversies. *Nat. Rev. Microbiol*, **2**, 820–832 (2004).
30. Šimek, M., Pekárek, S. & Prukner, V. Ozone Production Using a Power Modulated Surface Dielectric Barrier Discharge in Dry Synthetic Air. *Plasma Chem. Plasma Process*, **32**, 743–754 (2012).
31. Doležalová, E., Prukner, V., Lukeš, P. & Šimek, M. Stress response of Escherichia coli induced by surface streamer discharge in humid air. *J. Phys. D. Appl. Phys*, **49**, 075401 (2016).
32. Graves, D. B. The emerging role of reactive oxygen and nitrogen species in redox biology and some implications for plasma applications to medicine and biology. *J. Phys. D Appl. Phys. J. Phys. D Appl. Phys*, **45**, 263001–263042 (2012).
33. Pavlovich, M. J., Clark, D. S. & Graves, D. B. Quantification of air plasma chemistry for surface disinfection. *Plasma Sources Sci. Technol*, **23**, 065036 (2014).
34. Jeong, J., Kim, J. Y. & Yoon, J. The Role of Reactive Oxygen Species in the Electrochemical Inactivation of Microorganisms. *Environ. Sci. Technol*, **40**, 6117–6122 (2006).
35. Frederickson Matika, D. E. & Loake, G. J. Redox Regulation in Plant Immune Function. *Antioxid. Redox Signal*, **21**, 1373–1388 (2014).
36. Yu, H. *et al.* Effects of cell surface loading and phase of growth in cold atmospheric gas plasma inactivation of Escherichia coli K12. *J. Appl. Microbiol*, **101**, 1323–1330 (2006).
37. Sakiyama, Y., Graves, D. B., Chang, H. W., Shimizu, T. & Morfill, G. E. Plasma chemistry model of surface microdischarge in humid air and dynamics of reactive neutral species. *J. Phys. D. Appl. Phys*, **45**, 425201 (2012).

38. Machala, Z. *et al.* Formation of ROS and RNS in water electro-sprayed through transient spark discharge in air and their bactericidal effects. *Plasma Process. Polym*, **10**, 649–659 (2013).
39. Mai-Prochnow, A. *et al.* Atmospheric pressure plasmas: Infection control and bacterial responses. *Int. J. Antimicrob. Agents*, **43**, 508–517 (2014).
40. Montie, T. C., Kelly-Wintenberg, K. & Roth, J. R. An overview of research using the one atmosphere uniform glow discharge plasma (OAUGDP) for sterilization of surfaces and materials. *IEEE Trans. Plasma Sci*, **28**, 41–50 (2000).
41. Sykes, P. Introduction to Organic and Biochemistry. *Biochem. Educ*, **1**, 59 (1973).
42. Mittler, R. ROS Are Good. *Trends Plant Sci*, **22**, 11–19 (2017).
43. Mittler, R., Vanderauwera, S., Gollery, M. & Van Breusegem, F. Reactive oxygen gene network of plants. *Trends Plant Sci*, **9**, 490–498 (2004).
44. Erpen, L., Devi, H. S., Grosser, J. W. & Dutt, M. Potential use of the DREB/ERF, MYB, NAC and WRKY transcription factors to improve abiotic and biotic stress in transgenic plants. *Plant Cell. Tissue Organ Cult*, **132**, 1–25 (2018).
45. Hoang, X. L. T., Nhi, D. N. H., Thu, N. B. A., Thao, N. P. & Tran, L. S. P. Transcription Factors and Their Roles in Signal Transduction in Plants under Abiotic Stresses. *Curr. Genomics*, **18**, 483–497 (2017).
46. Seo, E. & Choi, D. Functional studies of transcription factors involved in plant defenses in the genomics era. *Brief. Funct. Genomics*, **14**, 260–267 (2015).
47. Iranbakhsh, A. *et al.* Non-thermal plasma modified growth and physiology in Triticum aestivum via generated signaling molecules and UV radiation. *Biol. Plant*, **61**, 702–708 (2017).
48. Jain, D. & Khurana, J. P. Role of pathogenesis-related (PR) proteins in plant defense mechanism. *Mol. Asp. Plant-Pathogen Interact*, 265–228 https://doi.org/10.1007/978-981-10-7371-7_12 (2018).
49. Noctor, G., Lelarge-Trouverie, C. & Mhamdi, A. The metabolomics of oxidative stress., **112**, 33–53 (2015).
50. Moon, U. R. & Mitra, A. A mechanistic insight into hydrogen peroxide-mediated elicitation of bioactive xanthones in Hoppea fastigiata shoot cultures., **244**, 259–274 (2016).
51. Filatova, I. *et al.* The effect of low-pressure plasma treatment of seeds on the plant resistance to pathogens and crop yields.*J. Phys. D. Appl. Phys.***53**, (2020).
52. Hoeben, W. F. L. M. *et al.* On the Possibilities of Straightforward Characterization of Plasma Activated Water. *Plasma Chem. Plasma Process*, **39**, 597–626 (2019).
53. Zhou, R. *et al.* Cold atmospheric plasma activated water as a prospective disinfectant: The crucial role of peroxynitrite. *Green Chem*, **20**, 5276–5284 (2018).
54. Guo, J. *et al.* Inactivation of Yeast on Grapes by Plasma-Activated Water and Its Effects on Quality Attributes. *J. Food Prot*, **80**, 225–230 (2017).
55. Guo, J. *et al.* F. L. Inactivation effects of plasma-activated water on Fusarium graminearum. *BioXriv*, https://doi.org/10.1101/2021.07.15.452455 (2021).

56. Perez, S. M. *et al.* Plasma activated water as resistance inducer against bacterial leaf spot of tomato. *PLoS One*, **14**, 1–19 (2019).
57. Adhikari, B., Adhikari, M., Ghimire, B., Park, G. & Choi, E. H. Cold Atmospheric Plasma-Activated Water Irrigation Induces Defense Hormone and Gene expression in Tomato seedlings. *Sci. Rep*, **9**, 16080 (2019).
58. ten Bosch, L., Köhler, R., Ortmann, R., Wieneke, S. & Viöl, W. Insecticidal Effects of Plasma Treated Water. *Int. J. Environ. Res. Public Health*, **14**, 1460 (2017).
59. Zhang, Q. *et al.* Sterilization Efficiency of a Novel Electrochemical Disinfectant against Staphylococcus aureus. *Environ. Sci. Technol*, **50**, 3184–3192 (2016).
60. Tarabová, B. *et al.* Fluorescence measurements of peroxynitrite/peroxynitrous acid in cold air plasma treated aqueous solutions. *Phys. Chem. Chem. Phys*, **21**, 8883–8896 (2019).
61. Aboubakr, H. A., Gangal, U., Youssef, M. M., Goyal, S. M. & Bruggeman, P. J. Inactivation of virus in solution by cold atmospheric pressure plasma: Identification of chemical inactivation pathways.*J. Phys. D. Appl. Phys.***49**, (2016).
62. Pavlovich, M. J., Chang, H. W., Sakiyama, Y., Clark, D. S. & Graves, D. B. Ozone correlates with antibacterial effects from indirect air dielectric barrier discharge treatment of water.*J. Phys. D. Appl. Phys.***46**, (2013).
63. Fang, J. *et al.* Non-thermal plasma-activated water inactivation of food-borne pathogen on fresh produce. *J. Hazard. Mater*, **300**, 643–651 (2015).
64. Glazebrook, J. Contrasting Mechanisms of Defense Against Biotrophic and Necrotrophic Pathogens. *Annu. Rev. Phytopathol*, **43**, 205–227 (2005).
65. Voráč, J., Synek, P., Procházka, V. & Hoder, T. State-by-state emission spectra fitting for non-equilibrium plasmas: OH spectra of surface barrier discharge at argon/water interface. *J. Phys. D. Appl. Phys*, **50**, 294002 (2017).
66. Voráč, J., Synek, P., Potočňáková, L., Hnilica, J. & Kudrle, V. Batch processing of overlapping molecular spectra as a tool for spatio-temporal diagnostics of power modulated microwave plasma jet. *Plasma Sources Sci. Technol*, **26**, 025010 (2017).
67. Voráč, J., Kusýn, L. & Synek, P. Deducing rotational quantum-state distributions from overlapping molecular spectra. *Rev. Sci. Instrum*, **90**, 123102 (2019).
68. Obrusník, A. *et al.* Electric field determination in air plasmas from intensity ratio of nitrogen spectral bands: I. Sensitivity analysis and uncertainty quantification of dominant processes. *Plasma Sources Sci. Technol*, **27**, 085013 (2018).
69. Filip, R. Gaussian quantum adaptation of non-Gaussian states for a lossy channel. *Phys. Rev. A*, **87**, 042308 (2013).
70. Bard, A. J. & Faulkner, L. R. Electrochemical Methods: Fundamentals and Applications, 2nd Edition. (John Wiley & Sons, Inc 2001).

71. Fernández, R. O. & Pizarro, R. A. Lethal effect induced in Pseudomonas aeruginosa exposed to ultraviolet-A radiation. *Photochem. Photobiol*, **64**, 334–339 (1996).
72. Kvam, E. & Benner, K. Mechanistic insights into UV-A mediated bacterial disinfection via endogenous photosensitizers. *J. Photochem. Photobiol. B Biol*, **209**, 111899 (2020).
73. Casadesús, J. & Low, D. Epigenetic Gene Regulation in the Bacterial World. *Microbiol. Mol. Biol. Rev*, **70**, 830–856 (2006).
74. Soni, A., Choi, J. & Brightwell, G. Plasma-activated water (PAW) as a disinfection technology for bacterial inactivation with a focus on fruit and vegetables. *Foods*, **10**, 1–13 (2021).
75. Mai-Prochnow, A. *et al.* Interactions of plasma-activated water with biofilms: inactivation, dispersal effects and mechanisms of action. *npj Biofilms Microbiomes*, **7**, 1–12 (2021).
76. Chen, T. P., Su, T. L. & Liang, J. Plasma-Activated Solutions for Bacteria and Biofilm Inactivation. *Curr. Bioact. Compd*, **13**, 59–65 (2016).
77. Zhou, R. *et al.* Microplasma Bubbles: Reactive Vehicles for Biofilm Dispersal. *ACS Appl. Mater. Interfaces*, **11**, 20660–20669 (2019).
78. Jiao, Y., Tay, F. R., Niu, L. & Chen, J. Advancing antimicrobial strategies for managing oral biofilm infections. *Int. J. Oral Sci*, **11**, 28 (2019).
79. Cherny, K. E. & Sauer, K. Untethering and Degradation of the Polysaccharide Matrix Are Essential Steps in the Dispersion Response of Pseudomonas aeruginosa Biofilms.*J. Bacteriol.***202**, (2020).
80. Bondarenko, A. S., Ragoisha, G. A. & Eis Spectrum Analyser. http://www.abc.chemistry.bsu.by/vi/analyser/ Available at: http://www.abc.chemistry.bsu.by/vi/analyser/.
81. Le Gorrec, B. & Montella, C. Handbook of Electrochemical Impedance Spectroscopy. Electrical Circuit Containing CPEs. Transformation 1–30(2010). doi:10.13140/RG.2.2.11979.62245
82. Pal, P. & Ghosh, A. Broadband dielectric spectroscopy of BMPTFSI ionic liquid doped solid-state polymer electrolytes: Coupled ion transport and dielectric relaxation mechanism. *J. Appl. Phys*, **128**, 084104 (2020).
83. Jonscher, A. K. A new understanding of the dielectric relaxation of solids. *J. Mater. Sci*, **16**, 2037–2060 (1981).
84. Munar, A., Andrio, A., Iserte, R. & Compañ, V. Ionic conductivity and diffusion coefficients of lithium salt polymer electrolytes measured with dielectric spectroscopy. *J. Non. Cryst. Solids*, **357**, 3064–3069 (2011).
85. Giampetruzzi, A. *et al.* Genome-Wide Analysis Provides Evidence on the Genetic Relatedness of the Emergent Xylella fastidiosa Genotype in Italy to Isolates from Central America. *Phytopathology®*, **107**, 816–827 (2017).
86. Goldman, E. & Green, L. H. Practical Handbook of Microbiology, Second Edition(CRC Press, Taylor and Francis Group, 2008).

87. Breed, R. and W. D. The Number of Colonies Allowable On Satisfactory Agar Plates. *J Bacteriol*, **1**, 321–331 (1916).

Figures

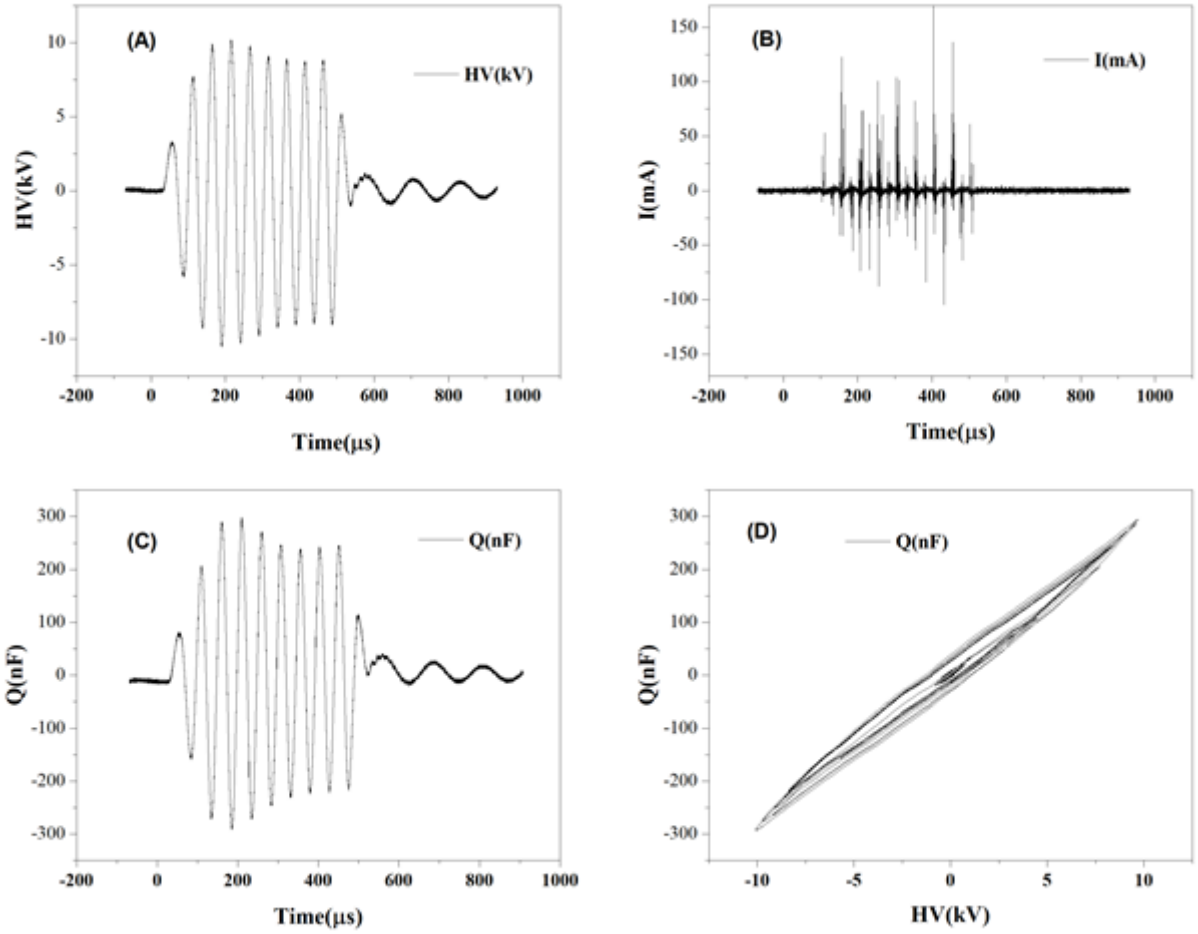

Figure 1

Typical waveform for 1 burst applied to the discharge reactor: (A) voltage; (B) current; (C) charge; (D) Lissajous figure for estimating the burst energy deposited in the plasma phase.

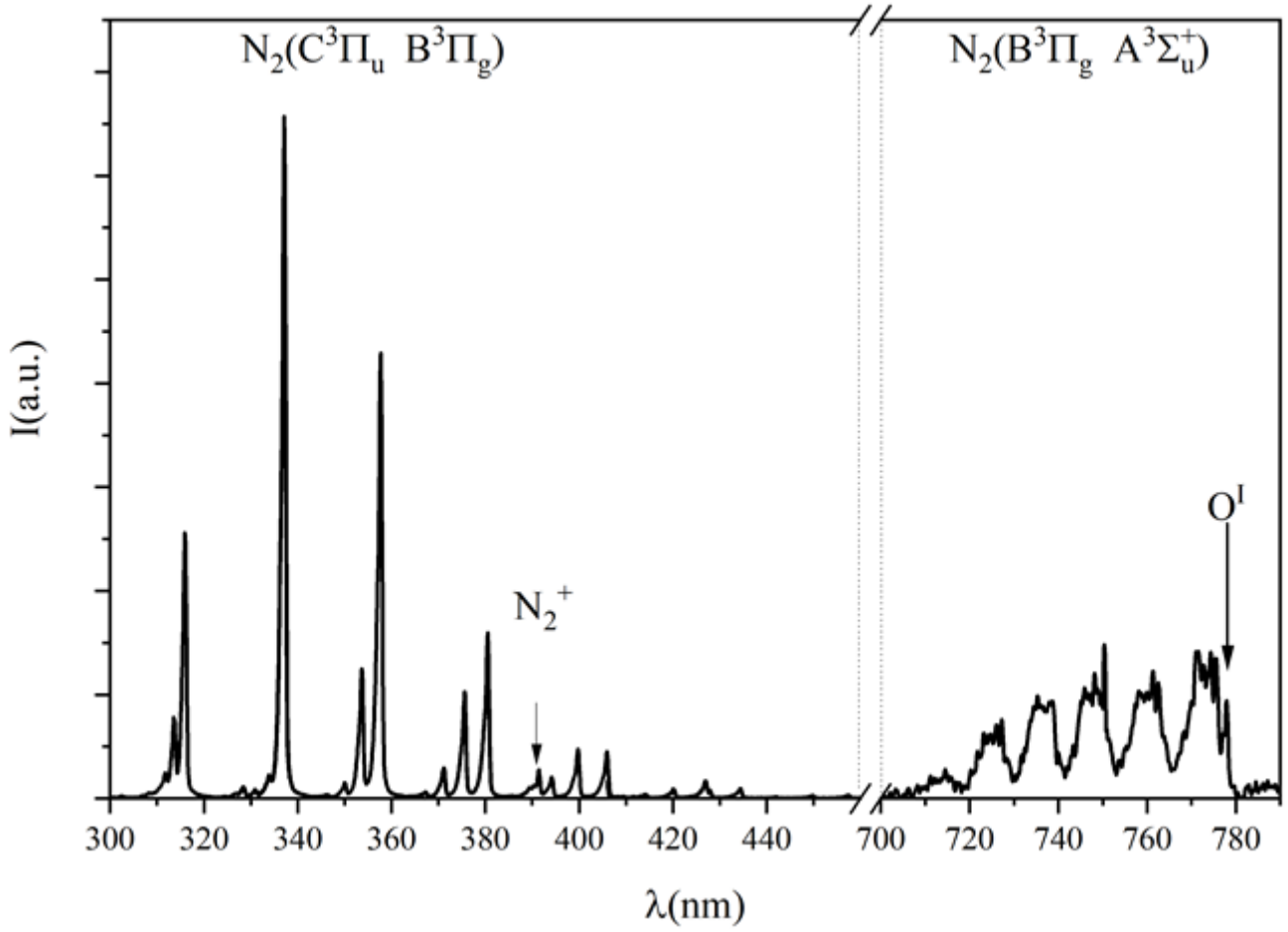

Figure 2

Typical averaged (1000 shots) electron impact induced emission over multiple discharge filaments developing over the entire ON time AC HV burst.

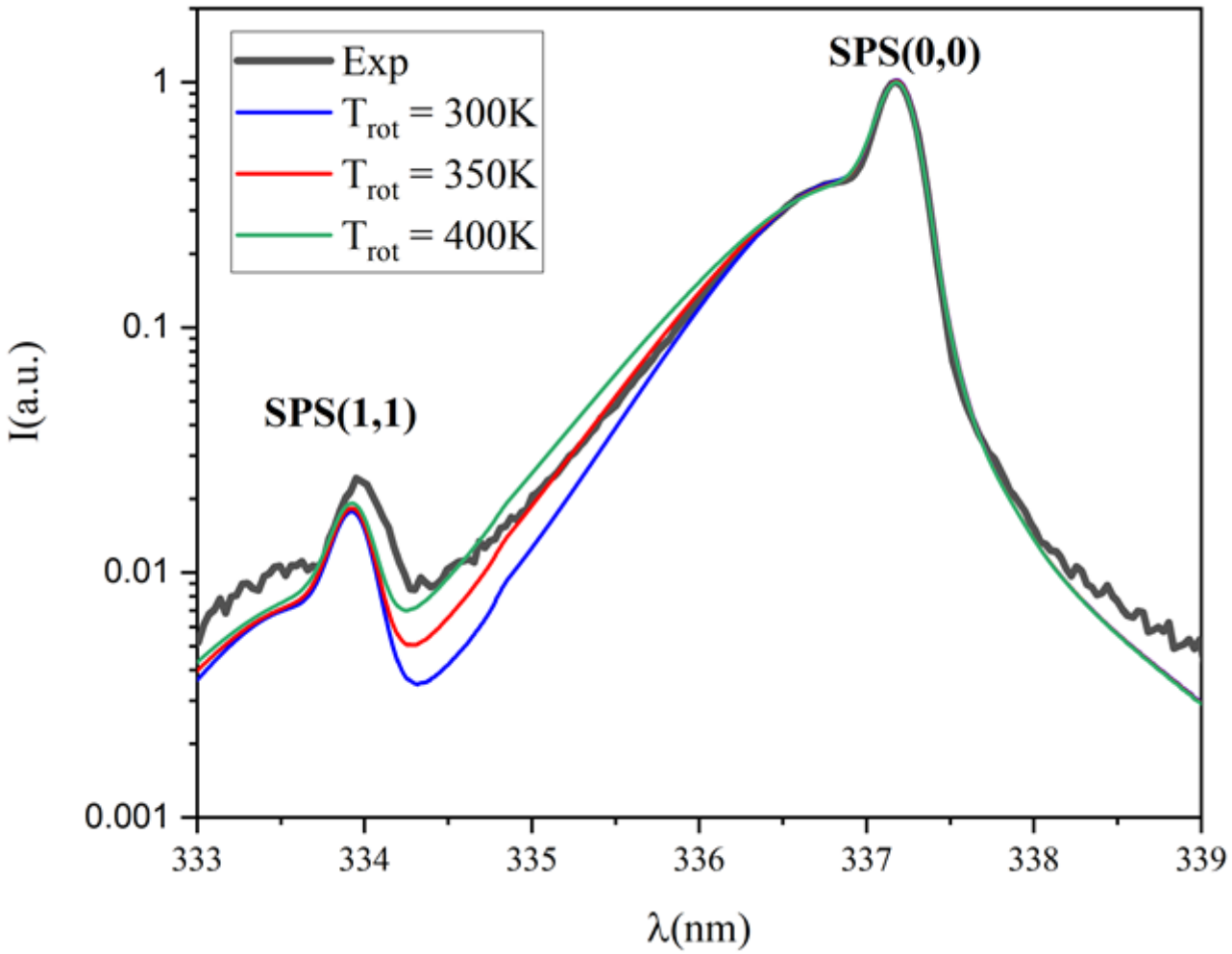

Figure 3

SPS(0,0) band emission (solid line) and simulated band profile for three different temperatures.

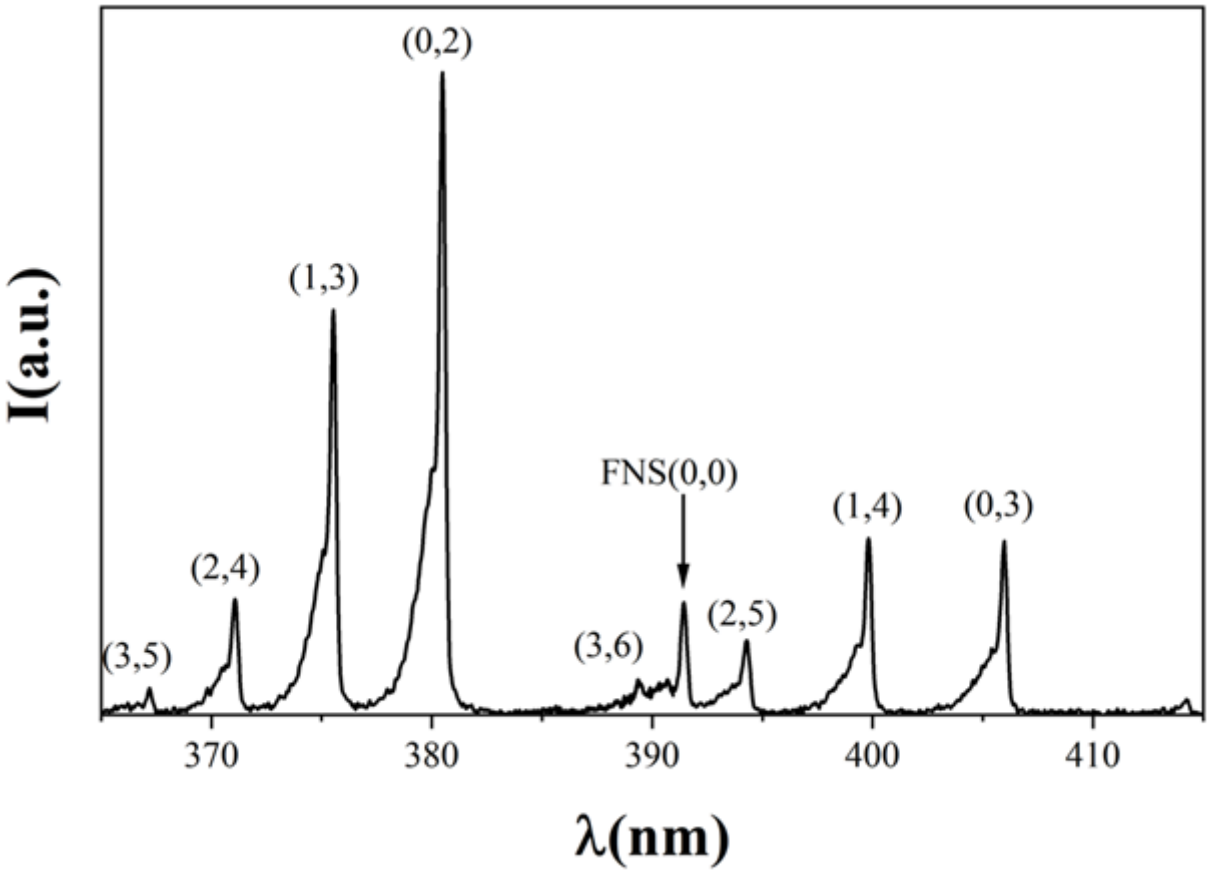

Figure 4

Emission Spectra of by the v = -3 and -2 sequences of the SPS and by v = 0 sequences of the FNS SPS

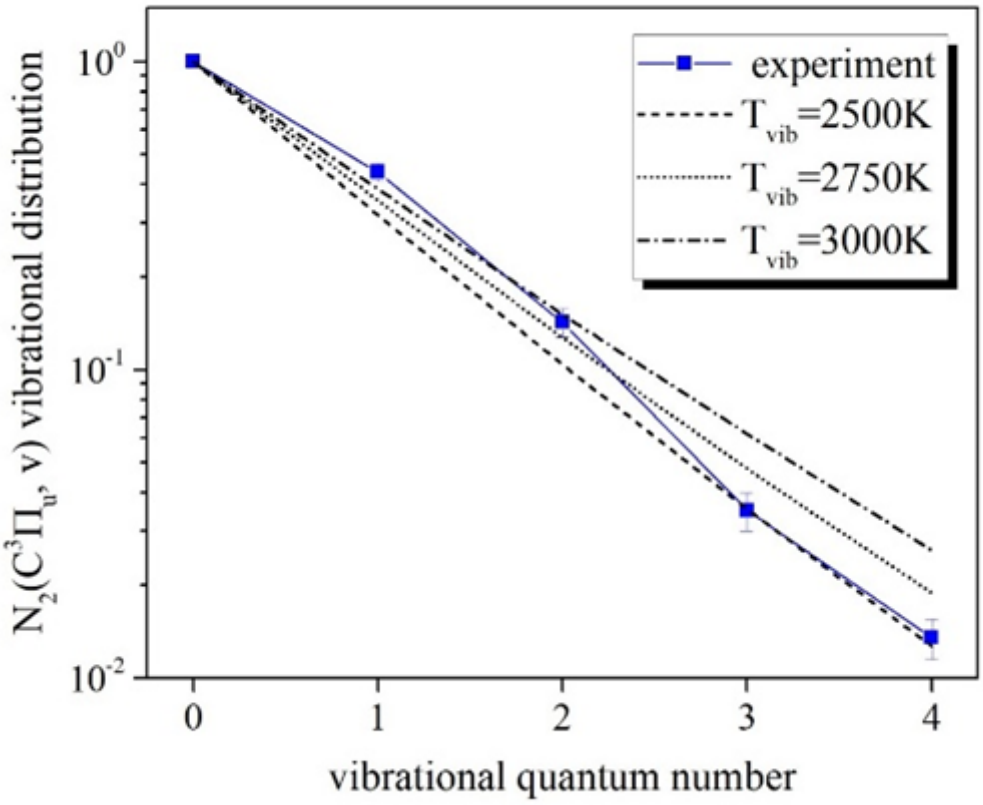

Figure 5

N2 C state vibrational distribution derived fom emission spectra of Figure 4.

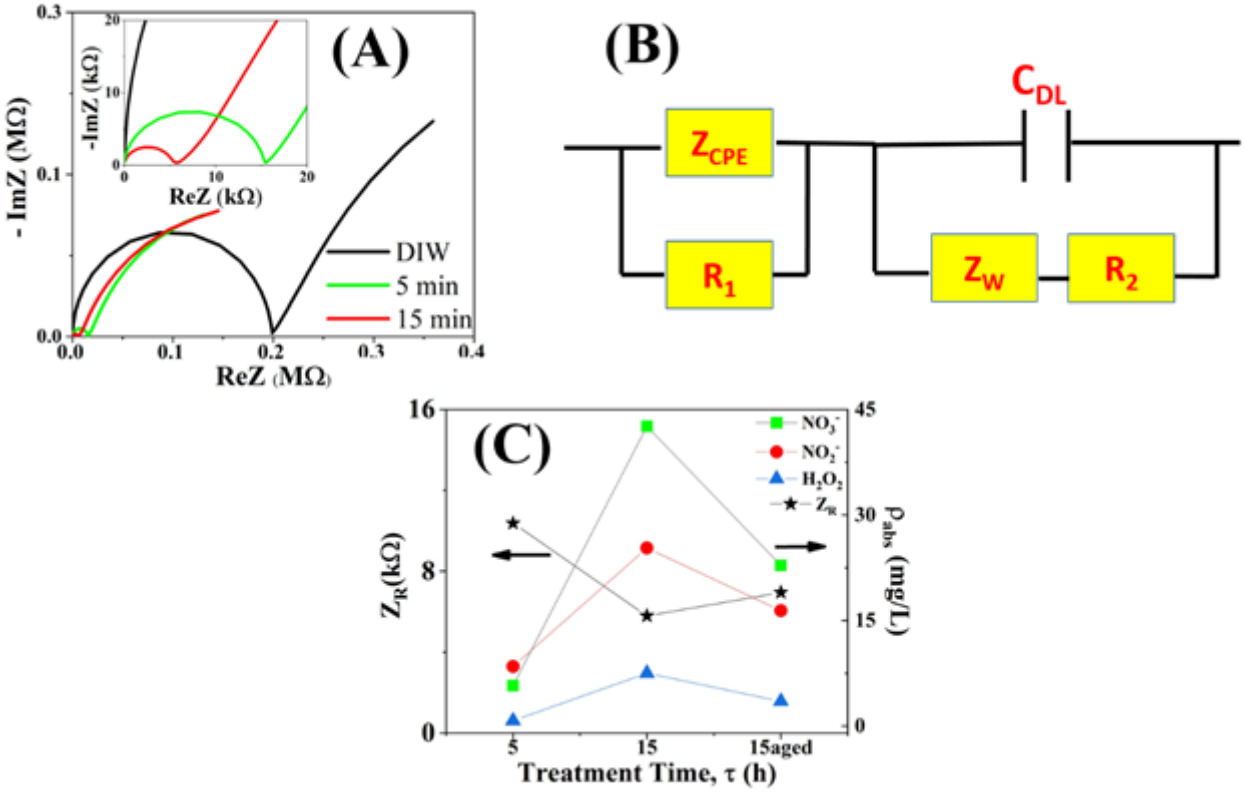

Figure 6

(A) Experimental NPs determined from the impedance measurements on PAW at two different treatment times T=5 min, 15 min. The NP of DIW is represented for comparison. The inset is an enlarged view of the f>100 Hz region. (B) The equivalent circuit used for the best fit of NPs in (A) (C) Impedance of the Randle circuit branch ZR = ZW+Rct as a function of the treatment time (left) and ionic species concentration as determined by optical absorption measurements. The increase/decrease of ZR corresponds to the decrease/increase of the ionic species concentration as determined by optical data.

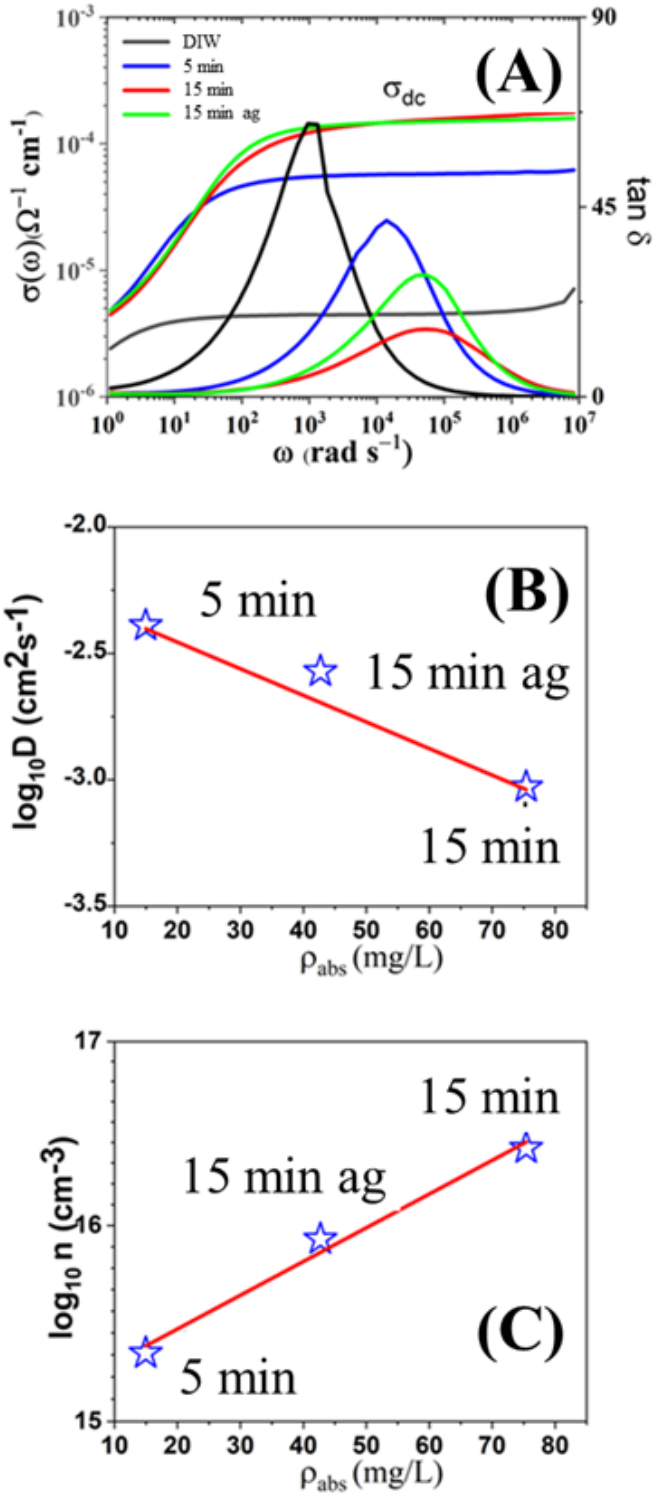

Figure 7

(A) AC conductivity (left y-axis) determined from impedance for DIW and PAW at two different treatment times and for the as-treated, 5 min, 15 min and the 15 min after 24 h (15 min ag); corresponding loss factor tan (right y-axis) for the same items. (B) Correlation between the ionic diffusivity D obtained by BDS and ionic species concentration abs via absorption data. For the calculation, we use the DC value at

the plateau at the angular frequency max (C) Correlation between ionic species obtained via optical absorption methods abs and BDS data, n.

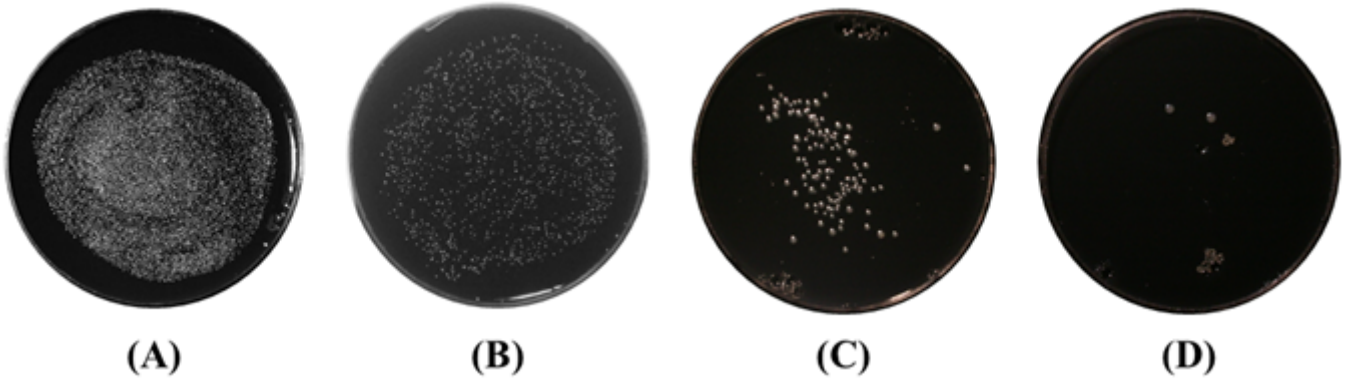

Figure 8

Time-dependent inhibition of XfDD growth by plasma exposure of cells discharged 1 day after plating. Photos were taken after 15 days post-exposure. The figure reports typical results for cells untreated (A) and treated for 10 (B), 100 (C), and 200 (D) s.

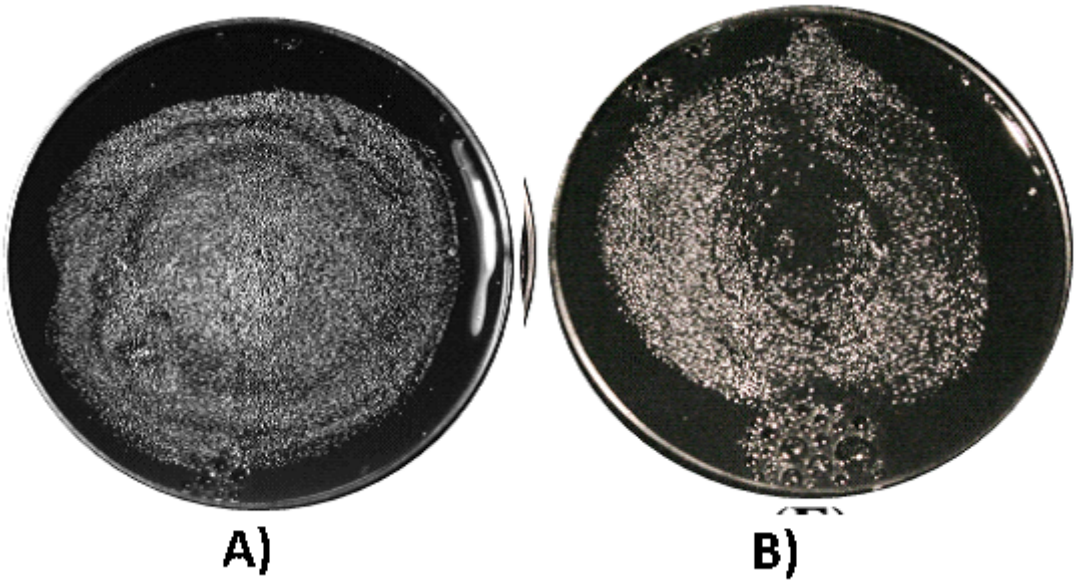

Figure 9

Effect of plasma treatment on XfDD strains (concentration 107) grown for 10 days (A) on the substrates before plasma treatment. Pictures were taken 15 days after plasma treatment. The picture shows the growth at 15 days from the plasma treatment of untreated samples (A) versus treated samples (B).

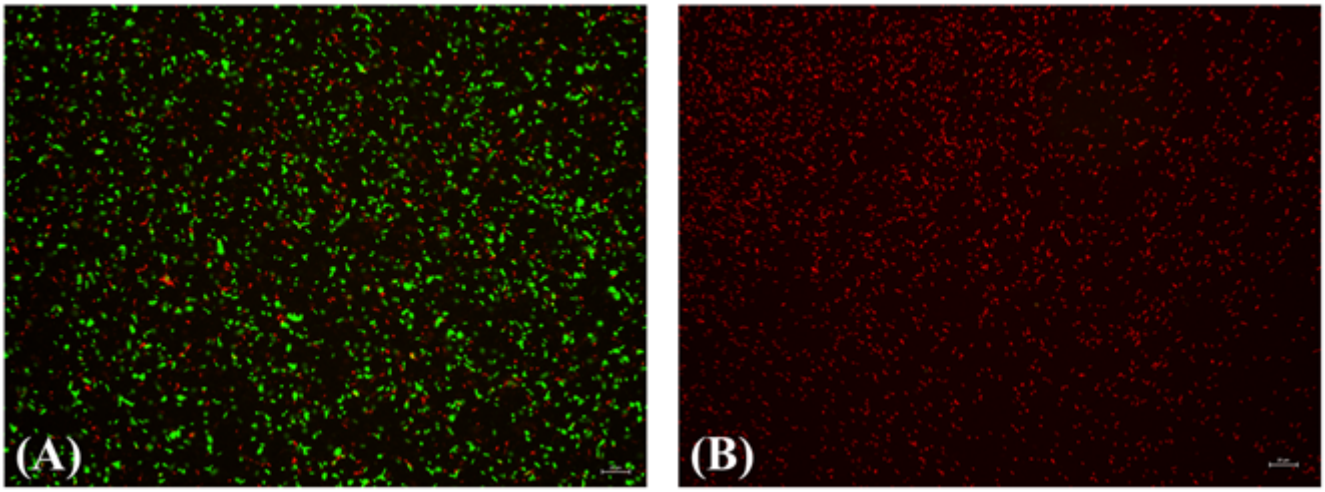

Figure 10

Fluorescence images of XfDD suspension in water for the untreated (A), and PAW treated (B) samples.